A Novel Application of Deformation Monitoring using GNSS-R Technology

Yang Yang, Yu Zheng, Wenkun Yu, Duojie Weng, Wenbin Li, Wu Chen

Department of Land surveying and Geo-informatics

Hong Kong Polytechnic University

Introduction

Global Navigation Satellite System Reflectometry (GNSS-R) has been first proposed in 1993 by M. Martin-Neira (Martin-Neira, 1993), as a promising technique for altimetry application. GNSS reflectometry involves having research on the GNSS signals, such as Global Positioning System (GPS) signal, both direct from the satellite and reflected from the object surface. Some characteristics of GNSS signal will alter due to the reflection. The characteristic changes are deemed to reflect some physical parameters of the object surface, which are expected to be able to calculate inversely by modeling the relationship between the direct and reflected signal.

Variety of applications have been developed and can be generally categorized into two groups: non-geometrical applications and geometrical applications. The non-geometrical applications are usually focusing on the amplitude or the power of the received signals. The applications include the sea state monitoring (Soulat et al., 2004), biomass monitoring (Ferrazzoli, Guerriero, Pierdicca, & Rahmoune, 2011), soil moisture (Egido et al., 2008) and snow depth (Jacobson, 2008) etc. The geometrical applications are focusing on the range difference of the direct and reflected signals. Depending on the GNSS signal structure and the application requirement, two types of altimetry algorithm have been researched: based on the code measurement and based on the carrier phase measurement. Due to the narrow bandwidth of code signal, the precision of code measurement might be relatively lower. However, it possesses the advantage of the capability to provide the range measurement over the rough or dynamic surface, like sea surface in windy weather. The precision of the several centimeters level in an average of a relatively long period of time (e.g. a few minutes) has been achieved using code altimetry by some researchers (Lowe et al., 2002) (Ruffini, Soulat, Caparrini, Germain, & Martín-Neira, 2004). A new approach called interferometric GNSS-R (iGNSS-R) has been developed by taking the direct signal for correlation,

instead of using locally generated code replica (Rius et al., 2012). The comparison result of both approaches has been presented by (Cardellach et al., 2014) in an airborne experiment, which shows that the iGNSS-R is at least two times better in precision than the traditional approach. In case of GPS, some researchers focused on the P-code for more precise range measurement due to higher chip rate (Lowe et al., 2002) (Mashburn, Axelrad, Lowe, & Larson, 2016). The carrier phase altimetry has been paid more attention for its better measurement performance, especially in static scenarios. Researches of carrier phase altimetry implemented on multiple platforms over various earth surfaces have been conducted over years, including lake surface monitoring from cliffs (Treuhaft, Lowe, Zuffada, & Chao, 2001) and from aircraft (Semmling, Beyerle, Beckheinrich, Ge, & Wickert, 2014), sea surface monitoring over bridges (Rivas & Martin-Neira, 2006) and sea ice monitoring by TechDemoSat-1 satellite (Li et al., 2017) (Hu, Benson, Rizos, & Qiao, 2017) etc.

A new application of slope deformation monitoring has been inspired by the remarkable achievements of GNSS-R altimetry and is proposed in this paper. Normally, the deformation monitoring can be achieved by multiple techniques, for ex ample conventional approaches (precise levelling, angle and distance measurement etc.), photogrammetric (aerial, satellite photogrammetry), positioning system (Global Position System) and radar system (InSAR), as well as some special techniques using laser ranger, tiltmeters, strainmeters etc. (Erol, Erol, & Ayan, 2004), depending on the surrounding environment and the budget. While developing the novel method of using GNSS-R for slope deformation monitoring possesses the advantages of low price, long-term, all-day all-weather and the capability of remote monitoring, which may expand the scope of the deformation monitoring application.

The traditional GNSS-R altimetry methods are not suitable to be applied to the deformation monitoring straightly. The deformation monitoring requires precise measurement result and relatively accurate spatial position of the monitoring object. And the environment might be complicated depending on the observation location and the target. To fulfill the requirements and meet the challenges, the carrier phase of the GNSS signal has drawn the attention due to its potential ability of precise measurement; the previous research of the application of GNSS-SAR (Zheng, Yang, & Chen, 2017) has been employed for the spatial position determination; and a geometry model has been applied to compensate the error caused by the environmental variation.

By taking the GPS signal as an example, the details of the algorithm of using GNSS-R for slope deformation monitoring are discussed in the next session.

The principle of using GNSS-R for deformation monitoring

The basic idea of using GNSS-R for slope deformation monitoring is to monitor the carrier phase of both direct and reflected signal, then retrieve the carrier phase difference as a representation of the slope deformation. The geometry of signal propagation is shown in figure 1. There are two different types of antenna involved: the right-hand circular polarization (RHCP) antenna for direct signal collection, and left-hand circular polarization (LHCP) antenna for reflected signal collection. Usually, the reflected signal power is much weaker due to the scattering. To ensure the signal tracking results are of acceptable quality, the receiver is normally placed close to the monitoring surface for stronger signal strength.

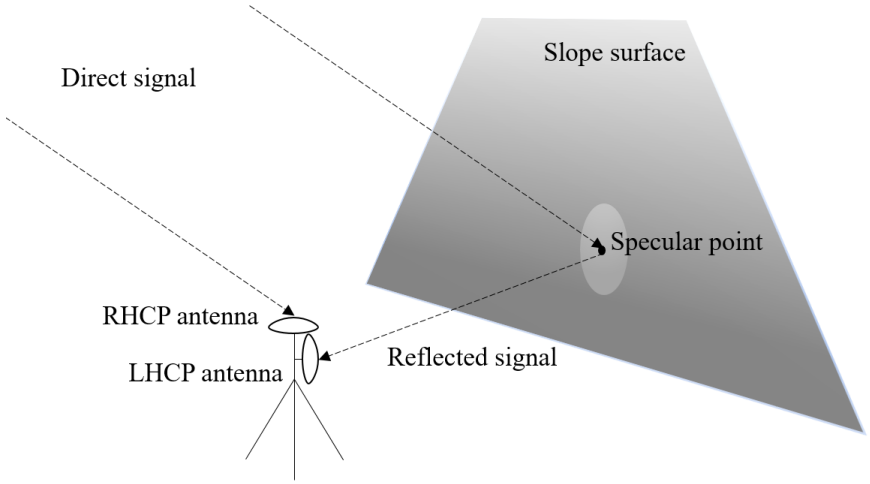

Figure 1. The geometry of using GNSS-R for slope deformation monitoring.

For the GPS satellite, the transmitted signal of the L1 band can be expressed as:

$$T(t) = A_T \cdot exp[i(\omega t + \varphi_L)] \cdot y(t) \cdot d(t) \quad (1)$$

Here, the term ωt represents the GPS signal carrier frequency. $\varphi_L$is the GPS signal carrier phase; $y(t)$ is the C/A code sequence; $d(t)$ is the GPS satellite navigation message.

When the signal arrives at the receiver, it can be expressed as the transmitted signal delayed by time τ and reduced in amplitude. In this case, the received direct signal can be expressed as:

$$R_d(t) = A_d \cdot exp[i(\omega(t-\tau_d) + \dot{\omega}(t-\tau_d) + \varphi_d)] \cdot y(t-\tau_d) \cdot d(t-\tau_d) + n \qquad (2)$$

Where τ_d is the time delay for the signal travelling from the transmitter to the direct antenna; the term $\omega(t-\tau_d)$ represents the signal carrier frequency, and $\dot{\omega}(t-\tau_d)$ represents the Doppler frequency caused by the relative movement between satellite and receiver; φ_d is the carrier phase of the received direct signal, which is corresponding to the signal transmitting time $t-\tau_d$; A_d is the amplitude of the direct signal when received, which contains all losses, including path losses and antenna losses etc.; n is the overall noise.

When the transmitted signal reaches and is reflected off the surface, due to the surface roughness, the signal is reflected from multiple facets surrounding the specular point, called glistening zone. Therefore, the received reflected signal is the combination of multiple reflected signals. However, in this close-range application of deformation monitoring, the glistening zone on a flat surface (shown as lighter color in figure 1) is quite small (Larson et al., 2009), and the reflected signal can be deemed to come from one indivisible resource. Therefore, the reflected signal can be expressed as:

$$R_r(t) = A_r \cdot exp[i(\omega(t-\tau_r) + \dot{\omega}(t-\tau_r) + \varphi_r)] \cdot y(t-\tau_r) \cdot d(t-\tau_r) + n \qquad (3)$$

Here, A_r represents the amplitude of the reflected signal, including all losses as same as the direct signal, plus the losses caused by extra propagation path and the surface scattering. The scattering loss may vary depending on the surface material and the roughness. τ_r is the time delay of the reflected signal regarding to the transmitted signal; φ_r is the reflected signal carrier phase; n is the overall noise. In this scenario, the navigation message $d(t)$ from the direct and reflected signal would be same, and the Doppler frequency difference would be negligible.

The range difference can be easily calculated if the direct and reflected signals are synchronized and steadily tracked. The carrier phase is chosen in this application for its potential ability of

precise measurement. The propagation path difference (Δd) between the direct and reflected signal is given by:

$$\Delta d = \varphi_d - \varphi_r = N\lambda + \varphi_\Delta \tag{4}$$

Here λ is the wavelength of GPS L1 signal, N is the integer number of wavelength, and φ_Δ is the fraction part of the carrier phase difference. If the environment is fixed, the propagation path difference will be a function that only depends on the satellite movement. When the observed target moves, there will be additional propagation path occurring and resulting in the carrier phase difference deviating from the original track.

To reveal the relationship between the deformation and the carrier phase difference of signals, a geometrical model has been developed referring to the previous work (Yu et al., 2017). The propagation path simulation of the direct and reflected signal is shown in figure 2. In the certain scenario, the satellite elevation angle (θ) and azimuth angle (α_s) can be calculated based on the satellite ephemeris data and the antenna position. The slope surface tilt angle (γ), azimuth angle (α_r) and the vertical distance between the antenna and the slope surface (d) can also be retrieved.

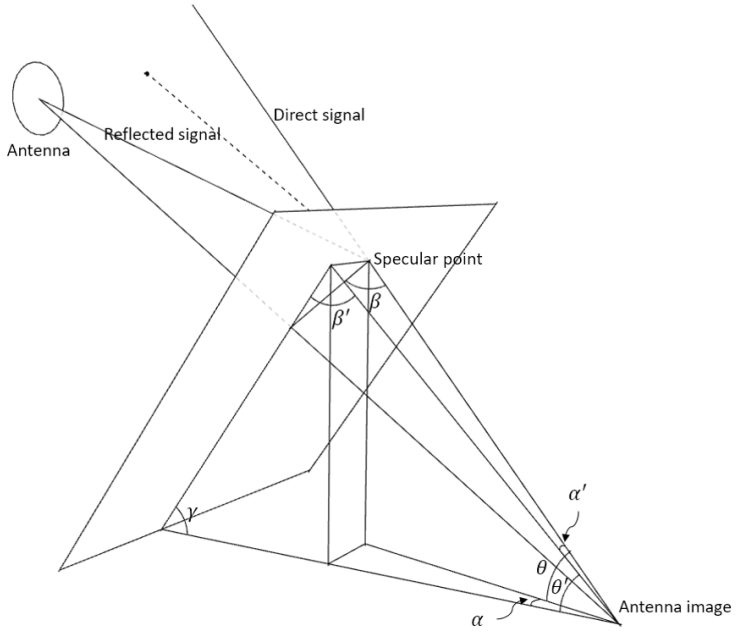

Figure 2. The signal reflection model

In this figure 2, the angle β is the equal to the signal incident angle and can be regarded as the equivalent elevation angle. And angle $\alpha = \alpha_s - \alpha_r$, is the difference between the azimuth angle of satellite and of the slope surface. And the angle θ' and β' are the projections of satellite elevation angle θ and equivalent elevation angle β on the front surfaces, respectively. The front surface is perpendicular to the ground and the slope surface. Hence, for the geometrical simulation, the propagation path difference (Δd) between the direct and reflected signal is given by:

$$\begin{cases} \Delta d = 2d \sin\beta \\ \sin\beta = \sin\beta' \cos\alpha' \\ \beta' = \pi - \theta' - \gamma \\ \tan\alpha' = \tan\alpha \cos\theta' \\ \tan\theta = \tan\theta' \cos\alpha \\ \alpha = \alpha_s - \alpha_r \end{cases} \tag{5}$$

There are two factors that influence the propagation path difference: the vertical distance between the antenna and the slope surface (d), and the equivalent elevation angle (β). The equivalent elevation angle β will change time to time due to the satellite movement. Hence, the propagation path difference (Δd) will not be a constant even there is no slope deformation occurring during the monitoring.

Before and after the deformation occurring, the carrier phase difference between direct and reflected signal is given by:

$$\begin{cases} \Delta d = 2d \sin\beta = N\lambda + \varphi_\Delta \\ \Delta d' = 2(d + d_{def}) \sin\beta' = N\lambda + \varphi'_\Delta \end{cases} \tag{6}$$

where, d_{def} is the deformation of the reflecting surface, along the normal direction; β and β' are the equivalent elevation angle before and after the deformation, respectively. And *N* is the carrier phase ambiguity. Assuming no circle slip occurred, due to the continuous observation, the ambiguity is same before and after the deformation.

For continuous monitoring, the changes of the carrier phase difference Δc should be:

$$\Delta c = \varphi_\Delta - \varphi'_\Delta$$

$$= \Delta d' - \Delta d = 2 \sin \beta \, (d - d') \quad (7)$$

Here, the term $d - d'$ represents the reflect surface deformation along the normal direction. Finally, the workflow of the slope deformation monitoring using GNSS-R can be given as figure 3.

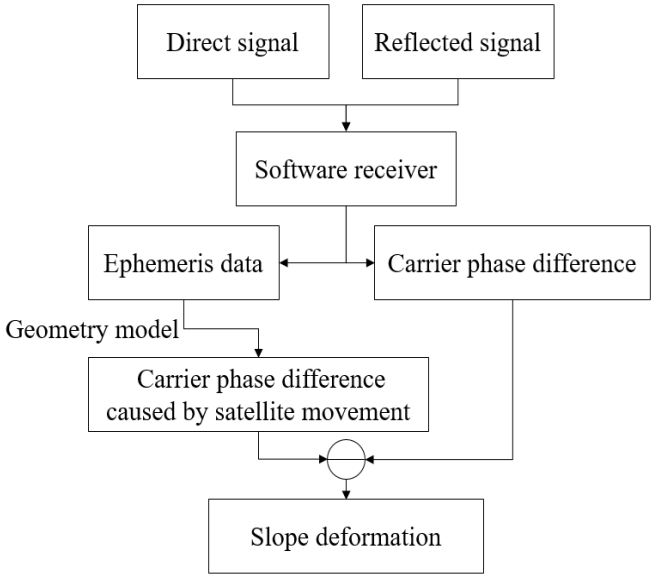

Figure 3. The workflow of slope deformation monitoring using GNSS-R

The front end and software receiver

To ensure the accurate results of carrier phase difference, the direct and reflected signals are required to be strictly synchronized. A custom-made dual-channel GPS/Galileo L1 radio frequency recorder was employed for signal collection. This front-end provides two parallel channels, which are synchronized by an oven-controlled crystal oscillator (OCXO) to eliminate the receiver clock error. Each channel can be considered as an independent front-end, which connects to a GPS antenna for the radio frequency (RF) signal collection. The structure of the front-end is shown in figure 4.

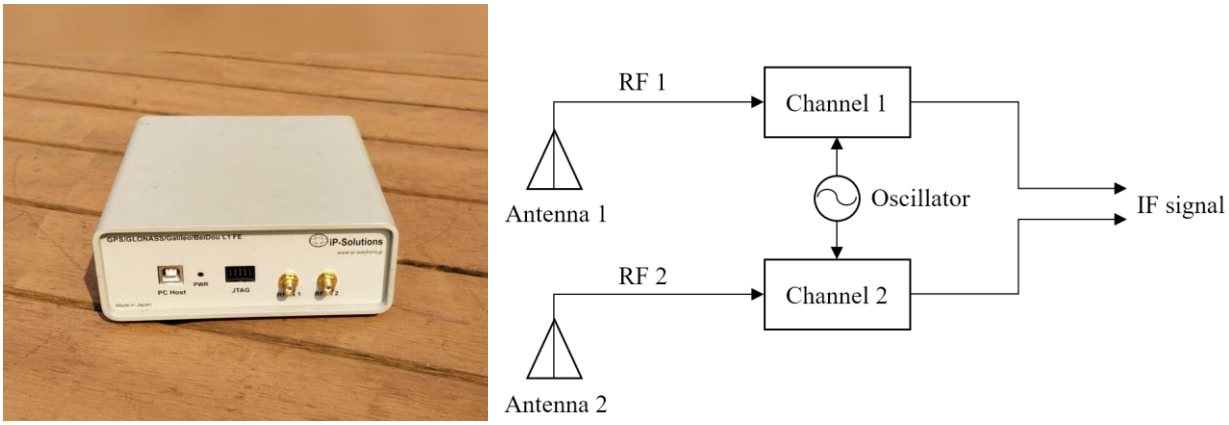

Figure 4. The iP-solutions GNSS-R front-end and its structure

The collected RF signal is down-converted to the intermediate frequency (IF) and then digitized and sampled. The device outputs 2-bit real-time data from each front-end channel. The RF recording software was installed on the host computer to manage the collection procedure. The IF stream data is delivered to the connected computer and stored on hard disk. The other specifications of the front-end are shown in table 1:

Antenna connector	SMA
Bandwidth (MHz)	4
Sampling rate (MHz)	16.368
Intermediate frequency (MHz)	4.092
Resolution	2 bits

Table 1. Specifications of iP-solutions front-end

A software receiver has been developed to process the synchronized dual-channel baseband signal. The normal IF signal processing flow is applied to each channel. There are two independent baseband signal processing modules. And the tracking results like carrier phase, pseudorange and Doppler frequency of each channel will be outputted. For further analysis, the pseudorange difference, carrier phase difference and Doppler frequency difference are also calculated. In the case of continuously monitoring, the change of the carrier phase difference between the direct and reflected signal is the most interested. The structure of the software receiver is shown in figure 5.

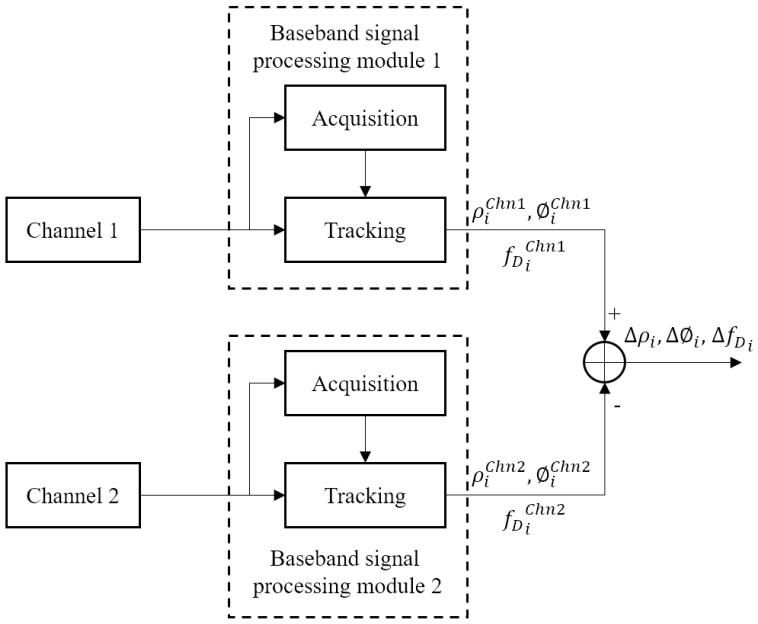

Figure 5. Structure of independent baseband signal processing

Experiment implementation and results

An experiment has been designed to simulate the environment of slope deformation and verify this algorithm. A slope near BLK Z, PolyU was chosen as the monitoring target. The slope tilt angle is about 40 degrees, and the azimuth angle is about 135 degrees from north. The receiver was installed on the rooftop of the BLK Z, facing to the slope, as shown in figure 6. Two antennas were installed on the tripod: the RHCP antenna was facing zenith to receive the direct signal and the LHCP antenna was facing to the slope to receive the reflected signal. Because it is difficult to find a slope in the progress of deformation for the experiment, the LHCP antenna was moved back and forth to simulate the deformation, while the RHCP antenna was set still. The LHCP antenna was moved 2 cm horizontally to simulate the deformation during the data collection.

Figure 6. The environment of experiment location at PolyU.

The GPS signals of PRN 2 and PRN 5 have been received simultaneously by both channels during the experiment. Depending on the position of GPS satellite, the specular point position on the slope varies correspondingly. ~~The GNSS-SAR images have been first processed to verify the specular point position. The image represents the power of the reflected signal from corresponding areas. The highlighted zone means the area which reflects higher power, and in this case, it indicates the position of the specular point.~~

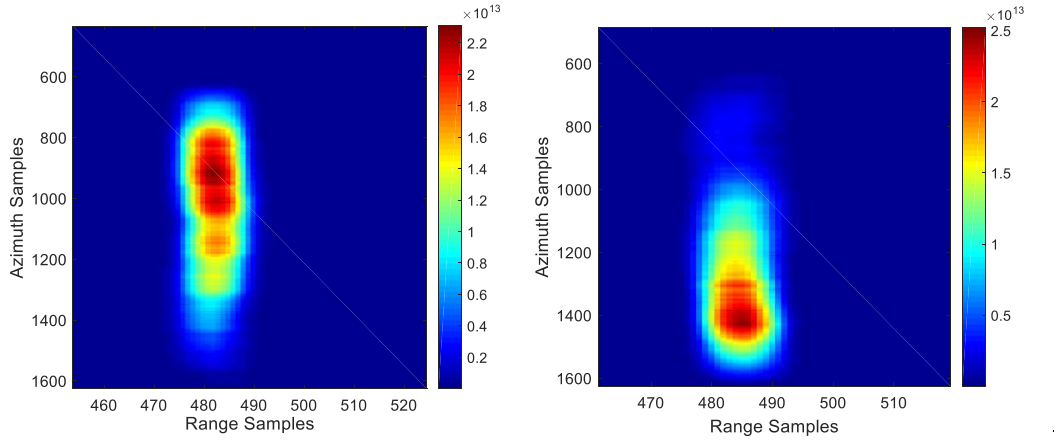

~~Figure 7. The GNSS-SAR images of PRN 15 (left) and PRN 29 (right)~~

~~As shown in figure 7, the range sample represents the distance along the range direction, which is the direction from the antenna to the reflector; and the azimuth sample represents the distance along the azimuth direction, which is along the slope and perpendicular to the range direction. 18 meters resolution in range direction has been achieved of the GNSS-SAR image. The resolution of range direction is relatively lower due to the low chip rate of C/A code. Whereas the azimuth~~

~~resolution reaches centimeters level for each pixel at the distance of 25 meters, which is considerably higher compared with the range resolution. The details of conducting the GNSS-SAR image can refer to the previous work (Zheng et al., 2017). In range direction, the positions of specular points corresponding to the signal of PRN 29 and PRN 15 are indistinguishable from the GNSS-SAR image. However, in the azimuth direction, it is obvious that the specular points are at different positions.~~

The received IF signals of both channels have been fed into the software receiver for signal acquisition and tracking. The carrier phase difference between the direct and reflected signal has been processed. To eliminate the carrier phase difference caused by satellite movement, the geometrical model has been applied to generate a simulation carrier phase difference, as shown in figure 8.

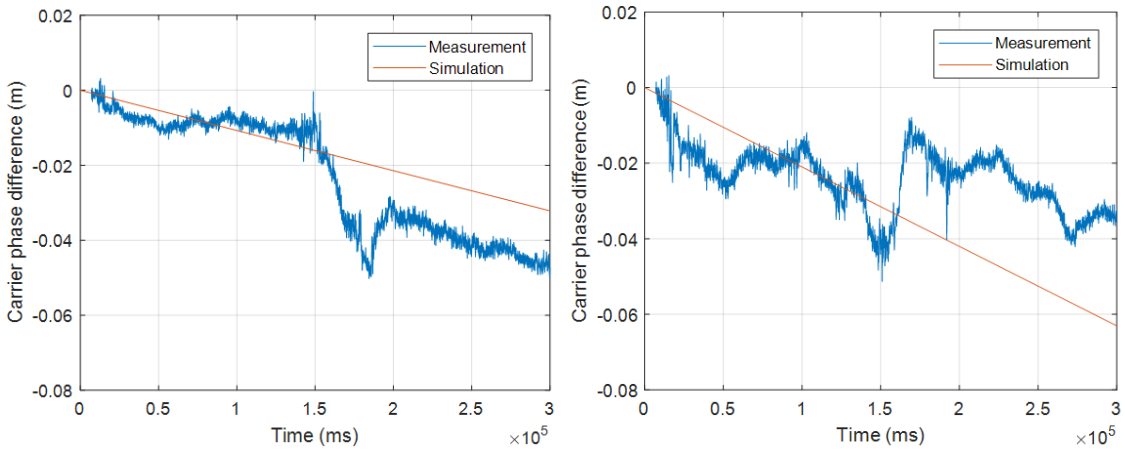

Figure 8. The comparison of measured and geometrical simulated carrier phase difference of PRN 2 (left) and PRN 5 (right).

Then the carrier phase difference caused by the deformation of the monitoring surface can be calculated by subtracting one from another, as shown in figure 9.

To eliminate the carrier phase difference error caused by the satellite movement, the time serials of the equivalent elevation angle of satellite PRN 15 and PRN29 have been calculated based on the geometry model. Then the deformation of the reflecting surface can finally be achieved.

Judging by the GNSS-SAR image and the outputted carrier phase difference, the reflected signal of PRN 15 seems not coming from the reflector but from the slope surface.

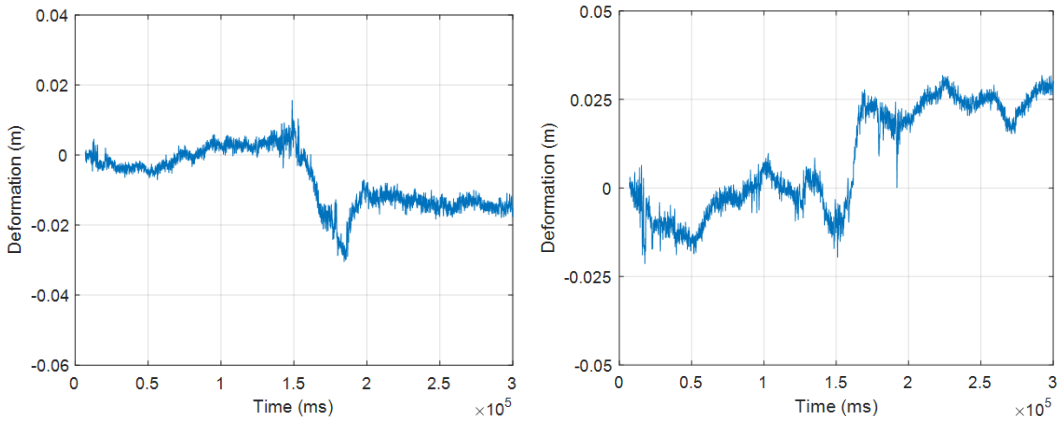

Figure 9. The deformation results of reflecting surface of PRN 2 (left) and PRN 5 (right).

The deformation outputted of PRN 15 shows no change during that time, which confirms the previous guess that signal was reflected from the slope surface. The deformation results fit nicely to the zero with the acceptable noise level. For the deformation results of PRN 29, a distinct leap shows at about 30 seconds, which represents the movement of the reflector. And the deformation value between the stable states of the beginning and ending is about 2 cm, which meets the movement distance of the reflector. The noise of the results of PRN 29 is noticeable larger compared with PRN 15, which might be caused by the vibration of the aluminum foil.

Conclusions

A novel application of GNSS-R is presented in this paper for slope deformation monitoring. The algorithm inspired by the GNSS-R altimetry has been discussed in detail. Other than directly retrieving the altimetry data, the more complicated and dynamic environment is the main challenge. The 3D geometrical model of signal reflection demonstrates the signal propagation and the factors that influence the path difference between the direct and reflected signal. Then the changes of carrier phase difference are linked to the slope deformation. The experiment of slope deformation monitoring has been designed to simulate the real-world scenario and to verify this algorithm. And the satisfying results have been achieved through the experiment.

The vulnerabilities of current algorithm lie in two aspects. The first is this method is only suitable the situation with one reflector, or single source reflected signal. In the situation of a more complicated environment, for example, the slope with an uneven surface, or surrounded by buildings, there might be multiple reflected signals coming from different resources, and the interference reflected signal will be received. Then the carrier phase of the received reflected signal is not equal to any of the signals. The second one is that this method requires continuous observation. If either of the signals is lost track, the carrier phase difference is meaningless. For current equipment, long time observation is impossible due to the data size. And the post processing algorithm restraints the possibility of real-time monitoring.

Reference

Cardellach, E., Rius, A., Martín-Neira, M., Fabra, F., Nogues-Correig, O., Ribo, S., . . . D'Addio, S. (2014). Consolidating the precision of interferometric GNSS-R ocean altimetry using airborne experimental data. *Ieee Transactions on Geoscience and Remote Sensing, 52*(8), 4992-5004.

Egido, A., Ruffini, G., Caparrini, M., Martin, C., Farres, E., & Banque, X. (2008). Soil moisture monitorization using GNSS reflected signals. *arXiv preprint arXiv:0805.1881*.

Erol, S., Erol, B., & Ayan, T. (2004). A general review of the deformation monitoring techniques and a case study: Analyzing deformations using GPS/leveling. Paper presented at the XXth ISPRS Congress.

Ferrazzoli, P., Guerriero, L., Pierdicca, N., & Rahmoune, R. (2011). Forest biomass monitoring with GNSS-R: Theoretical simulations. *Advances in space research, 47*(10), 1823-1832. doi:https://doi.org/10.1016/j.asr.2010.04.025

Hu, C., Benson, C., Rizos, C., & Qiao, L. (2017). Single-Pass Sub-Meter Space-Based GNSS-R Ice Altimetry: Results From TDS-1. *Ieee Journal of Selected Topics in Applied Earth Observations and Remote Sensing*.

Jacobson, M. D. (2008). Dielectric-covered ground reflectors in GPS multipath reception—Theory and measurement. *Geoscience and Remote Sensing Letters, IEEE, 5*(3), 396-399.

Larson, K. M., Gutmann, E. D., Zavorotny, V. U., Braun, J. J., Williams, M. W., & Nievinski, F. G. (2009). Can we measure snow depth with GPS receivers? *Geophysical Research Letters, 36*(17).

Li, W., Cardellach, E., Fabra, F., Rius, A., Ribó, S., & Martín‐Neira, M. (2017). First Spaceborne Phase Altimetry over Sea Ice Using TechDemoSat‐1 GNSS‐R Signals. *Geophysical Research Letters*.

Lowe, S. T., Zuffada, C., Chao, Y., Kroger, P., Young, L. E., & LaBrecque, J. L. (2002). 5‐cm‐Precision aircraft ocean altimetry using GPS reflections. *Geophysical Research Letters, 29*(10).

Martin-Neira, M. (1993). A passive reflectometry and interferometry system (PARIS): Application to ocean altimetry. *ESA journal, 17*, 331-355.

Mashburn, J., Axelrad, P., Lowe, S. T., & Larson, K. M. (2016). An Assessment of the Precision and Accuracy of Altimetry Retrievals for a Monterey Bay GNSS-R Experiment. *Ieee Journal of Selected Topics in Applied Earth Observations and Remote Sensing, 9*(10), 4660-4668. doi:10.1109/JSTARS.2016.2537698

Rius, A., Nogués-Correig, O., Ribó, S., Cardellach, E., Oliveras, S., Valencia, E., . . . van der Marel, H. (2012). Altimetry with GNSS-R interferometry: first proof of concept experiment. *GPS solutions, 16*(2), 231-241.

Rivas, M. B., & Martin-Neira, M. (2006). Coherent GPS reflections from the sea surface. *Ieee Geoscience and Remote Sensing Letters, 3*(1), 28-31.

Ruffini, n. G., Soulat, F., Caparrini, M., Germain, O., & Martín‐Neira, M. (2004). The Eddy Experiment: Accurate GNSS‐R ocean altimetry from low altitude aircraft. *Geophysical Research Letters, 31*(12).

Semmling, M., Beyerle, G., Beckheinrich, J., Ge, M., & Wickert, J. (2014). *Airborne GNSS reflectometry using crossover reference points for carrier phase altimetry.* Paper presented at the Geoscience and Remote Sensing Symposium (IGARSS), 2014 IEEE International.

Soulat, F., Caparrini, M., Germain, O., Lopez‐Dekker, P., Taani, M., & Ruffini, G. (2004). Sea state monitoring using coastal GNSS‐R. *Geophysical Research Letters, 31*(21).

Treuhaft, R. N., Lowe, S. T., Zuffada, C., & Chao, Y. (2001). 2‐cm GPS altimetry over Crater Lake. *Geophysical Research Letters, 28*(23), 4343-4346.

Yu, W., Ding, X., Chen, W., Dai, W., Yang, Y., (2017). Landslide monitoring based on multiple GNSS observations. Manuscript submitted for publication.

Zheng, Y., Yang, Y., & Chen, W. (2017). Enhanced GNSS-SAR Range-Doppler Algorithm for The Target Detection of Weak Reflected Signals: An Experimental Study. *Journal of Aeronautics, Astronautics and Aviation, 49*(2), 83-92.